Wiley

Zero-Standby Power Hydrogen Sensing Using Event-Driven Micromechanical Switches

S M Jahadun Nobi, Eric Herrmann, Zhixiang Huang, Sai Rahul Sitaram, Kyle Laskowski, and Xi Wang*

S M Jahadun Nobi, Eric Herrmann, Zhixiang Huang, Sai Rahul Sitaram, Kyle Laskowski, Xi Wang

Department of Materials Science and Engineering, College of Engineering, University of Delaware, Newark, DE 19716, USA

E-mail: wangxi@udel.edu

Keywords: Zero standby power, Event-driven detection, Hydrogen gas sensor, Palladium, Passive switch, Hydrogen detection

Zero-standby power sensors are crucial for enhancing the safety and widespread adoption of hydrogen (H₂) technologies in chemical processes and sustainable energy applications, given the flammability of H₂ at low concentrations. Here, we report an event-driven hydrogen sensing system utilizing Palladium (Pd)-based micromechanical cantilever switches. The detection mechanism relies on strain generation in the Pd layer, which undergoes reversible volume expansion upon hydrogen adsorption. Our experimental and simulation results demonstrate that the bistable micromechanical switch-based sensor generates a wake-up signal with activation time depending on hydrogen concentration in the target environment while always remaining active for events without any standby power consumption under normal conditions. The H₂ adsorption-induced subsequent switching of the multi-cantileverbased switch configuration on the sensor resulted in the quasi-quantification of hydrogen concentrations. The reported zero-standby power sensor's operational lifetime is limited by the frequency of detection events and exposure to concentrations exceeding hydrogen's flammability limit. This work advances the development of high-density, maintenance-free sensor networks for large-scale deployment with Internet of Things devices, enabling unattended continuous monitoring of hydrogen generation, transportation, distribution, and end-user applications.



1. Introduction

The global community is making progress in combating climate change by prioritizing greenhouse gas reduction, promoting renewable energy adoption, and strengthening international cooperation. [1] Hydrogen (H₂), a carrier of green energy, is one of the initiatives to help this effort by offering a pathway to achieve the goal of net-zero greenhouse gas emissions, as fossil fuels contribute 80-90% of global greenhouse gas emissions. [2] H₂, with its high energy density [3] and clean combustion, [4] has found increasing applications in recent years, including domestic heating, transportation, [5, 6] chemical, [7] biological, [8] and medical fields. [9, 10] However, its low-energy ignition, buoyancy, and rapid flame propagation in air raise significant safety concerns. [5, 11] Therefore, to advance toward a net-zero emissions future by promoting hydrogen as a green energy source, researchers face the critical challenge of developing systems for leak detection and concentration measurement. Moreover, these systems must function independently with minimal maintenance, be employed in large numbers across vast regions, including remote and hard-to-reach areas, particularly where hydrogen leakage is rare.

Hydrogen sensors have evolved significantly over time, utilizing various materials and detection mechanisms. The interaction between hydrogen and sensitive materials forms the basis for these sensors, with commonly utilized sensing materials including palladium (Pd), [12, ^{13]} platinum (Pt),^[11] various metal oxides such as ZnO,^[14] SnO₂,^[15] TiO₂,^[16] WO₃,^[17] as well as nanomaterials (e.g., reduced graphene oxide (rGO), carbon nanotubes (CNTs))[18-23] and composite materials.^[24] Pd is particularly favored due to its high hydrogen absorption properties. The underlying detection mechanisms that the above-mentioned sensing materials use can be broadly categorized as catalytic, thermal conductivity, electrical/electrochemical, mechanical, optical, or acoustic. [5, 12, 25-27] However, many of these detection mechanisms require elevated temperatures and biasing conditions, which increase system complexity and power consumption. This limitation makes them less suitable for widespread deployment, especially in scenarios where the occurrence of the target event is rare.^[5] Although acoustic H₂ sensors are compact and energy-efficient, they struggle with long-term stability and selectivity. These issues can affect their reliability in continuous monitoring applications. [23, ^{28]} In contrast, optical sensing techniques provide high specificity and rapid signal transmission but are constrained by size, complexity, and the high costs associated with largescale instrumentation. [5, 29] Consequently, although each sensor type exhibits unique merits and limitations, they all suffer from high power consumption, regular maintenance, or

deployment costs, which hampers their suitability for widespread, low-maintenance applications.

Duty-cycled sensing technology can significantly solve the power consumption issues of the existing H₂ sensors. However, in contrast to continuous scanning, where a sensor persistently waits for a signal of interest to trigger an alert and consistently depletes batteries through ongoing electronic operations, the duty-cycled sensors could miss target events during inactive periods and result in data fidelity issues.^[20, 30] Therefore, the constant standby power consumption of battery-powered sensors, even with duty cycling, hinders the scalability of sensor networks; specifically, in terms of the number of deployable sensors, as well as regular maintenance due to the need for frequent battery replacements, along with the associated hardware and labor costs.[31] An event-driven, always active, zero-standby power consumption sensing technique has recently been proposed to power large-scale unattended sensor networks. [32-34] In this approach, sensors harvest vibrations, [34] electron tunneling, [35] and electromagnetic radiation energy^[36] emitted from the target of interest and use it as a specific signature to trigger a switch. The development of event-driven H₂ sensing technology, in which sensors work passively without consuming any power until triggered by a specific H₂ exposure event, has the potential to revolutionize H₂ sensing technology as well as boost the transition towards a H₂-based economy. To the best of our knowledge, no prior demonstrations can reliably monitor H₂ leakage without depleting batteries, underscoring the necessity of a true zero-standby power H₂ sensing platform for the advancement of a net-zero hydrogen future.

In this study, we present a novel Pd-based micromechanical bistable switch for hydrogen detection. The switch, consisting of two physically separated electrodes, remains continuously responsive to target signals without consuming power during standby conditions and operates in an event-driven manner. Activation occurs only when the ambient hydrogen concentration exceeds a defined threshold. Unlike conventional logic devices, which suffer from leakage currents even in the off state, the bistable switch based on micro- and nanoelectromechanical (MEM/NEM) relays exhibit extremely low leakage and steep subthreshold slopes by leveraging their structure, resulting in a true zero standby power switching system. [37-39] The reported switch-based sensor nodes can be deployed within a grid network, as conceptually illustrated in Figure 1a. A base station communicates with the distributed sensor nodes using radio frequency signals. It collects local atmospheric data and transmits alerts and relevant

information when a target event is detected. The sensor node architecture with the switch as a key element is illustrated in Figure 1b. The mechanical actuation triggers the switching mechanism, which activates auxiliary electronics and the broader sensing system only upon hydrogen detection. This design choice of a simplified switch rather than providing a continuous quantitative measurement is motivated by the specific objective of leak detection. Hydrogen leaks are infrequent, but each event requires immediate detection and response. Therefore, a quasi-quantitative approach that confirms the presence of a leak is sufficient, particularly in large-scale sensor deployment applications where minimizing cost is important. In addition, a simplified switch-based design enhances system consistency and reliability. It can also be integrated with existing miniaturized sensing systems that are commercially available. [40, 41] Therefore, the platform presented in this work offers a deployable and scalable solution for H₂ gas sensing, with low operational and maintenance costs, making it well-suited for large-scale, high-resolution sensing networks.

2. Design and Simulation

The designed H₂ actuated switches consist of anchored cantilevers with freely moving tips and a bottom contact region, as illustrated in Figure 2a. Each cantilever serves as a hydrogenresponsive moving electrode, while the bottom contact region works as a fixed electrode. The structure is designed to ensure that the cantilever remains flat in normal conditions, allowing the moving electrode to contact the fixed electrode in the target environment. A U-shaped cantilever design was selected as it offers a balanced combination of sensitivity, structural stiffness, electrical performance, and dynamic tunability.^[42-44] Copper (Cu), chromium (Cr), ruthenium (Ru), and Pd are used for the cantilever design, with Pd as the top layer and Ru as the tip. The Ru tip was selected for its advantageous material properties, such as low contact resistance, minimal material transfer during cycling, resistance to carbon contamination, and excellent mechanical and thermal stability under both hot and cold switching conditions. These properties collectively enable reliable and repeatable contact performance over extended operation. [45] The thickness of each layer is optimized using a see-saw method to achieve a moderately flat cantilever with a slight upward curvature. [46] Upon H₂ adsorption, the Pd layer expands while the underlying layers retain their original volume, bending the cantilever downwards. This structural change of the microcantilever enables the activation of the designed switching mechanism. The sensor system consists of four independent cantilever switches of lengths 50, 75, 100, and 125 µm connected in parallel during the measurement steps, to facilitate the quasi-quantification process. Each cantilever is designed with a specific

surface-to-volume ratio, and its length determines the separation distance between its movable tip and the bottom fixed electrode.

Numerical simulation using COMSOL Multiphysics was performed to evaluate the switching mechanism of the H₂-actuated microcantilever. A 3D model with mirror operation was employed to simplify the processes, as it allows for a more manageable computational load while maintaining the system's essential features. Considering the mechanical boundary condition, this model simulates the Cr/Cu/Cr/Pd tetra-layered microcantilever switch with a Ru tip. A fixed constraint was applied to the anchor of the cantilever structure. To simulate the effect of hydrogen absorption, the adsorption-based stress formation was used. [29, 47] The initial stress and strain values for the materials used in the cantilever are available in the references.^[46, 48, 49] The stress generated in Pd thin films during deposition is compressive and varies with film thickness.^[48] With all these parameters, the curvature of the cantilever before and after the hydrogen adsorption could be predicted. The detailed simulation results shown in Figure 2c and Figure 2d illustrate the von Mises stress under normal environmental conditions and the displacement of the cantilever at a 1% H₂ concentration following H₂ absorption, respectively. These results reveal that the maximum von Mises stress is distributed in the anchor area of the cantilever beam, while the maximum displacement occurs at the free end. A detailed description of simulations is provided in the Supporting Information.

3. Fabrication

The fabrication process of the hydrogen-actuated switches includes forming a fixed bottom electrode with Pt and creating a Pd-based cantilever structure with a Ru tip. The device described herein was fabricated at the University of Delaware Nanofabrication Facility, utilizing five maskless microfabrication processes in conjunction with standard nanofabrication techniques, including multiple depositions and dry etching.

A 1-inch×1-inch thermal oxide substrate served as the basis for the device fabrication. Given that the etchant employed for the release process of the microcantilever switch must be highly selective regarding the structural materials of the device, i.e., Cu, Cr, Pd, Pt, and SiO₂, gas or plasma etchants are preferred over wet etchants, as they more effectively mitigate the risk of stiction. ^[50] Consequently, germanium (Ge) was selected as the sacrificial material to address this requirement. Two distinct dry etching processes were developed to etch the Ge. The first

process utilized sulfur hexafluoride (SF₆) gas to dry etch the Ge film anisotropically, achieving a steep side profile. This etching process was optimized to attain high selectivity between the materials employed in the device and the Ge sacrificial layer, which was crucial for the precise definition of the narrow gaps and structural features of the device. The second dry etching process, based on fluorine based inductively coupled plasma (FICP), utilized carbon tetrafluoride (CF₄) gas for isotropic etching of the Ge sacrificial layer and was optimized to ensure high selectivity towards the Ge material while exerting minimal to no adverse effects on the properties of all the other cantilever materials.

The fabrication process eliminates the need for hydrofluoric acid (HF) etching, ^[46] and supports a more environmentally sustainable approach. In addition, these dry etching processes protect the cantilever materials by avoiding exposure to the HF-based wet etching process. The Supporting Information (Figure S2) provides a detailed description of the fabrication steps, along with corresponding illustrations. Figure 2b shows a scanning electron microscopy (SEM) image of a fabricated hydrogen-actuated switch. The SEM image indicates that the U-shaped cantilever beams are suspended and exhibit upward deflection, attributed to the stress gradient within the Cr and Pd layers. The distance between the U-shaped movable cantilever tip and the bottom fixed electrode was measured to be approximately 3.3, 7.1, 13.1, and 19.8 µm for cantilever lengths of 50, 75, 100, and 125 µm, respectively, with minimal variation observed during repeated fabrication. Following the completion of the microcantilever switch release process, the fabricated device was wedge-bonded to a chip carrier for subsequent characterization.

4. Results and Discussion

The zero-standby power sensors were tested using H₂/N₂ mixtures at hydrogen concentrations of 1%, 2%, and 5% to evaluate the sensor's performance to varying concentrations, facilitating a quasi-quantification of hydrogen concentration. A customized sensor test system was built to characterize the devices as illustrated in Figure 3a. The system comprises a test chamber, an electrical response measurement system, and a gas supply system. The test chamber, with a volume of 180 cm³, is constructed from acrylic and features a polished fused quartz spectroscopic window. This window enables continuous monitoring of microcantilever displacement in the target environment using long-working-distance objectives in a probe station. During the measurement process, a selected gas mixture was introduced into the test chamber via a three-way valve. A flow regulator controlled the gas flow to maintain laminar

flow conditions within the chamber. After each measurement, the chamber was purged with pure N_2 gas to observe the sensor's on-to-off transition process. The wedge-bonded device was securely positioned inside the test chamber, connected to the electrical test equipment via wires. Sensor measurements were conducted by applying a DC voltage of 10 mV using a source meter with a current limit of 1 μ A. The electrical outputs were continuously monitored and recorded in real time using a Python script. The first meter measured the current flow through the device, while the second meter recorded the voltage drop across it. Additionally, the second meter can be triggered by the wake-up signal generated when current flows through the first meter. All experiments were conducted at room temperature under laboratory conditions.

The connection diagram to collect the electrical output for a single cantilever in the tested device is shown in Figure 3b. In this configuration, the wake-up signal is generated when the actuated cantilever contacts the bottom electrode, completing the circuit and allowing current to flow from the moving electrode to the fixed electrode or vice versa. The resistance R_1 and R_2 functioned as current-limiting components to prevent thermal damage to the bistable cantilever-based switch.

The results of a sensor tested in a 1% H_2 environment balanced with N_2 are presented in Figures 4a and 4b. As anticipated, the device showed reversible transition from the off-state to the on-state when the Pd layer absorbed H_2 , causing the cantilever to bend downward and complete the switching process. During this off-to-on transition, the current increased from a near-zero value to approximately 400 nA, generating a wake-up signal capable of initiating data acquisition and activating auxiliary electronics. Concurrently, the voltage dropped from an open-circuit value of 10 mV to approximately 190 μ V after establishing contact. The actuation time for the off-to-on transition was measured to be 26 ± 1 minutes under the 1% hydrogen condition. When the hydrogen flow was discontinued and only N_2 was introduced into the chamber, the palladium layer released the absorbed hydrogen. This desorption allowed the cantilever to return to its original position, restoring the off state. The open-circuit voltage returned to 10 mV, and no current flow was observed, confirming the reversibility and stability of the bistable switching behavior under repeated operation.

To further assess the sensor's performance under varying target environments, both the current and corresponding voltage drop across the device were measured for H₂

concentrations of 1%, 2%, and 5% in N₂ carrier gas using the same sensor. In each case, the sensor system generated a wake-up signal following H₂ exposure. The actuation time is defined as the duration between the initial exposure to H₂ and the generation of the wake-up signal. For the 1% H₂ concentration, the actuation time was consistent with the results mentioned in the earlier paragraph. At higher concentrations, the off-to-on switching occurred more rapidly, requiring 15.5 ± 0.5 minutes for 2% H₂ and 4 ± 1 minutes for 5% H₂, as shown in Figures 4c and 4d, respectively. The transition from on to off state was initiated by discontinuing the hydrogen flow and introducing nitrogen into the chamber. In all tested cases, the current dropped to zero within 3 ± 0.5 minutes, indicating that the switch returned to its off state. The presence of a physical gap between the device terminals is expected to enable very high off-state resistance and a large on-to-off current ratio.^[32] However, the resolution of the multimeter used in the experimental setup prevented precise measurement of the off-state current. Even when increasing the applied voltage from 10 mV to 1 V, the measured standby current remained below 1 nA. This implies that the actual off-state current is well below 10 pA, corresponding to a standby power consumption of less than 100 fW. Optical microscopy observations confirmed that the switch required additional time to fully return to its initial position after H₂ desorption. These results demonstrate that a completely passive, zero-standby-power platform can be accomplished using the H₂-actuated bistable switch. The transition between two stable states reliably occurs after the sensor absorbs and desorbs H₂ for a duration that depends on the concentration, thereby satisfying key requirements for low-power hydrogen detection and monitoring systems.

To evaluate the quasi-quantification capability of the sensor system, we analyzed the voltage drop across the multi-cantilever sensor configuration under varying H₂ environments. The temporal voltage response for two such responses with 1% and 5% H₂ concentrations is shown in Figures 5a and b, respectively. Following the generation of the wake-up signal, i.e., the first switching event, the measured voltage across the switches undergoes a transient stabilization period of approximately 3 seconds. The measured voltage then stabilizes once a firm contact is established between the electrodes. As H₂ continues to flow into the chamber, additional independent switches in the multi-cantilever system engage sequentially, leading to changes in the measured voltage across the device. This behavior arises because of the design of all the initial upward bending independent cantilevers to traverse different distances to engage the contact points. While the current remains nearly constant due to the presence of high-value current-limiting series resistors, the voltage drops across the device exhibited a

reduction of more than 50% from its initial value due to additional switching events caused by the reduction of the total resistance of the multi-cantilever sensor system. For a 1% H₂ concentration, the second switching event occurred 100.5 seconds after the first (Figure 5a), while for a 5% H₂ concentration, it occurred after 12 seconds (Figure 5b). Additionally, a third switching event was detected at the higher hydrogen concentration, further evident in the 5% H₂ in N₂ environment shown in Figure 5b.

We analyzed the relationship between consecutive switching events under varying hydrogen concentrations to further investigate the quasi-quantification capability of the multi-cantilever sensor system. The correlation between the first and second switching events for 1% and 2% H₂ concentrations is presented in Figure 6a and b, respectively. In both cases, five devices from the same fabrication batch were tested to minimize inconsistencies arising from fabrication variability, and each device was exposed to H₂ multiple times. Repeated testing revealed that the first switching time exhibited slight variations due to the inherent hysteresis associated with the hydrogen adsorption and desorption process, as described by the phase transition process provided in the Supporting Information. Linear regression analysis was performed on the experimental data. For 1% H₂ concentration, the regression equations were found to be $t_2 = t_1 + 104.5 \pm 5.1$, with a coefficient of determination (R²) of 0.75. For 2% H₂ environment, the equation was $t_2 = t_1 + 84.1 \pm 4.8$ with R^2 value of 0.86. Both equations suggest an uncertainty of approximately 5 seconds in the offset parameter, reflecting the effect of noise and experimental variability. Additionally, the 95% prediction band encompassed all data points, confirming that the output of sensors provides a statistically reliable estimate of the second switching time after the first. This suggests a consistent temporal relationship between switching events, with deviations captured by the offset parameter. This correlation is significant because the system does not record the absolute time of the first switching event following hydrogen leakage. Instead, the timing mechanism begins only after the generation of the initial wake-up signal. Therefore, the device estimates hydrogen concentration based on the time interval between independent switching events. This behavior enables a practical zero-standby power hydrogen detection and quasiquantification system, where energy consumption occurs only during active sensing events.

One critical aspect of the presented device architecture is using Pd as the sensing layer.

Although Pd and its alloys remain among the most widely used materials for hydrogen detection due to their high catalytic activity and exceptional hydrogen solubility, Pd exhibits

intrinsic hysteresis during the α to β phase transition, as described in the Supporting Information. ^[12, 51, 52] This behavior poses a limitation to long-term sensor stability. Our experiment indicates that the cantilever-based sensor undergoes plastic deformation when subjected to higher hydrogen concentrations in 5% H₂ in balanced N₂. This deformation arises from phase transition-induced stress and leads to performance degradation after three or four operational cycles under 5% H₂ concentration, ultimately compromising the device's ability to generate a reliable wake-up signal and subsequent switching for the quasi-quantification process.

Material-oriented approaches, such as alloying palladium with other elements or forming palladium compounds, can lower the activation energy for hydrogen absorption, reduce or eliminate phase hysteresis, and achieve faster response with higher sensitivity. [53, 54] Replacing the palladium layer with such engineered materials is therefore a promising route to improve both durability and overall sensing and actuation performance of the device. [12, 55]

Furthermore, reported results, as also supported by our simulation results in Figure S1, reducing the electrode separation within the switch structure can accelerate actuation by minimizing the required cantilever displacement. [56] Addressing these material and structural challenges through targeted alloy selection and geometric refinement will be crucial for advancing this technology toward practical, reliable, and fully passive hydrogen sensing applications.

Compared to the presented sensor, most commercially available H₂ sensors exhibit power consumption ranging from 2 mW to 4 W, making them impractical for large-scale, maintenance-free IoT deployments.^[11] Recent advancements in Pd-based resistive, capacitive, and optical hydrogen sensing have focused on enhancing sensitivity and response time and have achieved rapid responses and parts-per-million level sensitivity.^[26, 27, 57] However, they typically consume power in the microwatt to milliwatt range for continuous monitoring.^[11, 12, 47, 56, 58, 59] Moreover, many of these sensing platforms rely on external readout circuits or optical components that add to the overall energy demand and hinder their integration into a compact sensor network.^[12, 56, 58] In contrast, the demonstrated bistable switch-based sensor achieves passive actuation and operates without standby power, offering a scalable and energy-efficient solution for H₂ leak detection with minimal maintenance needs.



5. Conclusion

We have demonstrated a zero-standby power, bistable switch-based sensor system that combines hydrogen detection and quasi-quantification within a single passive MEMS, leveraging palladium's unique hydrogen absorption properties. The sensor exhibited a reversible off-to-on transition in response to varying hydrogen concentrations, with activation times dependent on H₂ levels. The device successfully generated a wake-up signal of ~400 nA, triggering an external system for data collection and alarm purposes. Switching actuation times were recorded as 26 ± 1 minutes for 1% H₂, 15.5 ± 0.5 minutes for 2% H₂, and 4 ± 1 minutes for 5% H₂ after the initial wake-up signal, providing quasi-quantification. The system's off-to-on state transition, facilitated by a physical gap between terminals, ensures minimal to no power consumption when inactive. It plays a critical role in developing miniaturized smart sensor microsystems, enabling passive monitoring to support the transition toward a hydrogen-based economy. Its fully passive operation, reliable switching behavior, and scalable design make it well-suited for real-world applications in energy, safety, and environmental monitoring with an extended operational lifetime. The system is ideal for unattended deployments that require long-term monitoring of infrequent yet time-sensitive hydrogen leaking events. The system concept may be adapted for detecting other volatile chemical compounds by incorporating alternative sensing materials, instead of Pd used here, that undergo lattice expansion or shrinkage in response to specific target environments. Future work will focus on enhancing response times, improving sensitivity at lower hydrogen concentrations, and minimizing hysteresis at high hydrogen concentrations, towards devices in practical applications.

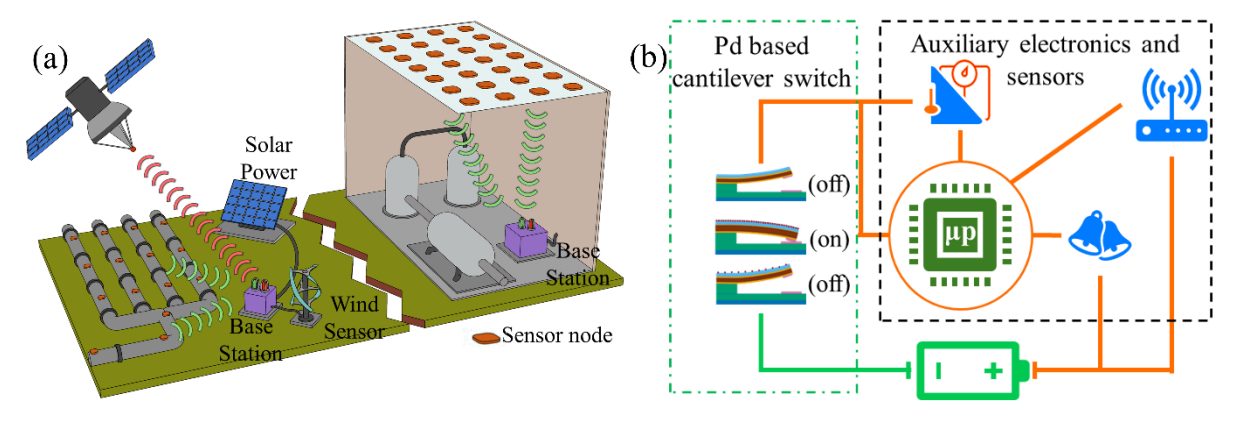
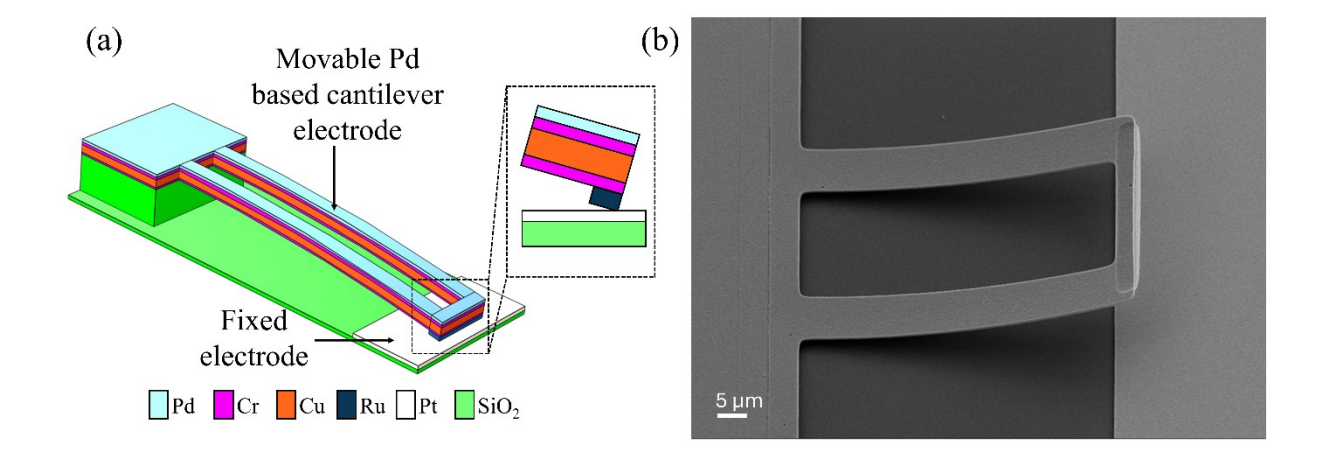


Figure 1: (a) The conceptual illustration of a zero-standby power sensor network intended for both outdoor and indoor environments where sustainable, wide-area coverage with minimal upkeep is needed. In this system, sensor nodes communicate with a central base station using RF signals. The base station includes RF communication modules, control units, and data analysis components. It collects data from the sensor nodes, incorporates local atmospheric measurements, and issues alarms and leakage notifications when a leak is detected. (b) The overall sensor node architecture. Pd-based microcantilever serves as the fundamental sensing unit within each sensor node. When exposed to H₂, the Pd layer on the microcantilever absorbs the gas and undergoes volumetric expansion. This expansion induces mechanical deformation in the microcantilever, causing it to bend downward and close the gap between the moving and stationary electrodes. Upon H₂ desorption, the Pd layer contracts, allowing the cantilever to revert to its initial position. This mechanical action connects the battery to the auxiliary electronics and sensors, e.g., temperature, humidity, and wind sensors, and thus triggers the alert system.



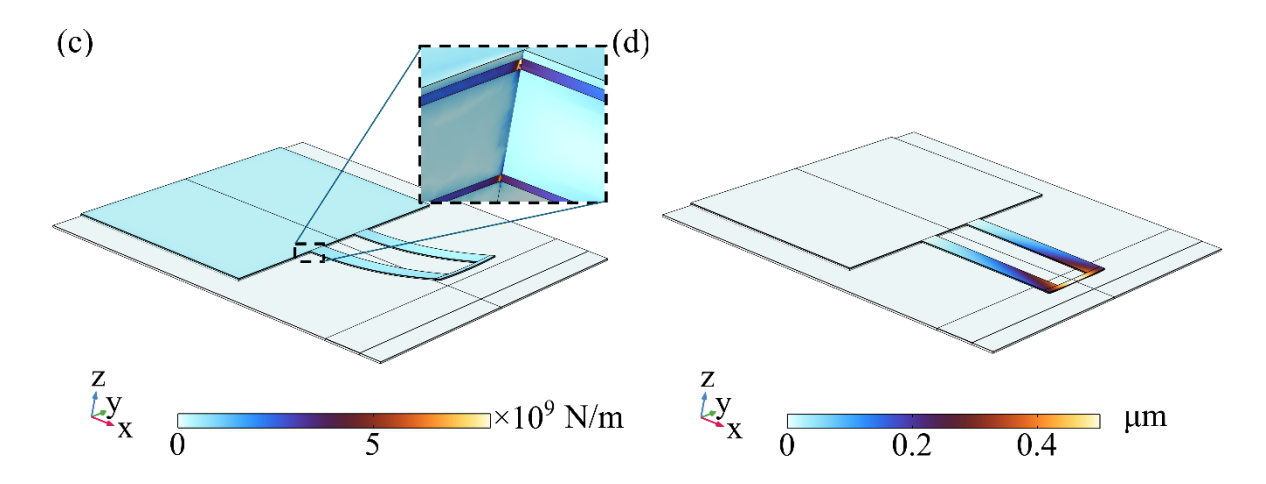


Figure 2: (a) Schematic of the Pd-based microcantilever switch. (b) SEM image of a fabricated Pd-based microcantilever switch. Finite Element Method (FEM) analysis of a 75 μ m long U-shaped cantilever switch: (c) von Mises stress distribution in an air environment, (d) vertical displacement of the cantilever at 1.0% H₂ in balanced N₂ environment. Residual stress causes the microcantilever to bend upward after fabrication, and it bends downward upon hydrogen adsorption.

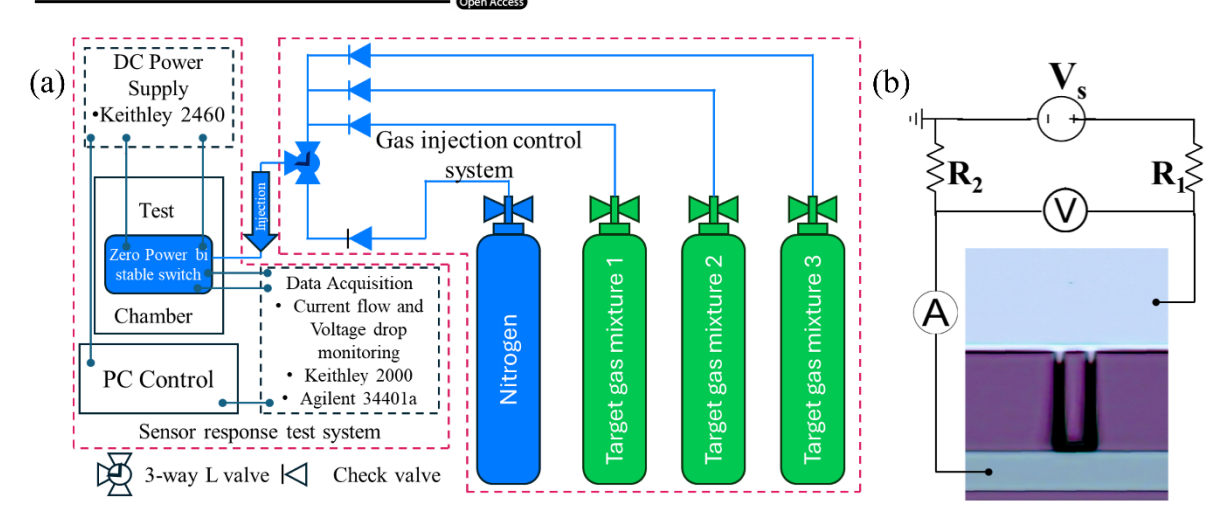


Figure 3: Schematic diagram of the experimental configuration. (a) The in-house gas test system. A regulator is used to select one of the specific concentrations of target gases, which are supplied to the test chamber through a flow regulator. (b) Circuit diagram of a single microcantilever in the sensor system. The system input voltage is applied between the moving and bottom electrodes. When the cantilever switch bends downward and closes the gap, current flows through the moving electrode to the fixed bottom electrode. R_1 and R_2 are the current limiting resistances to protect the cantilever from high current.

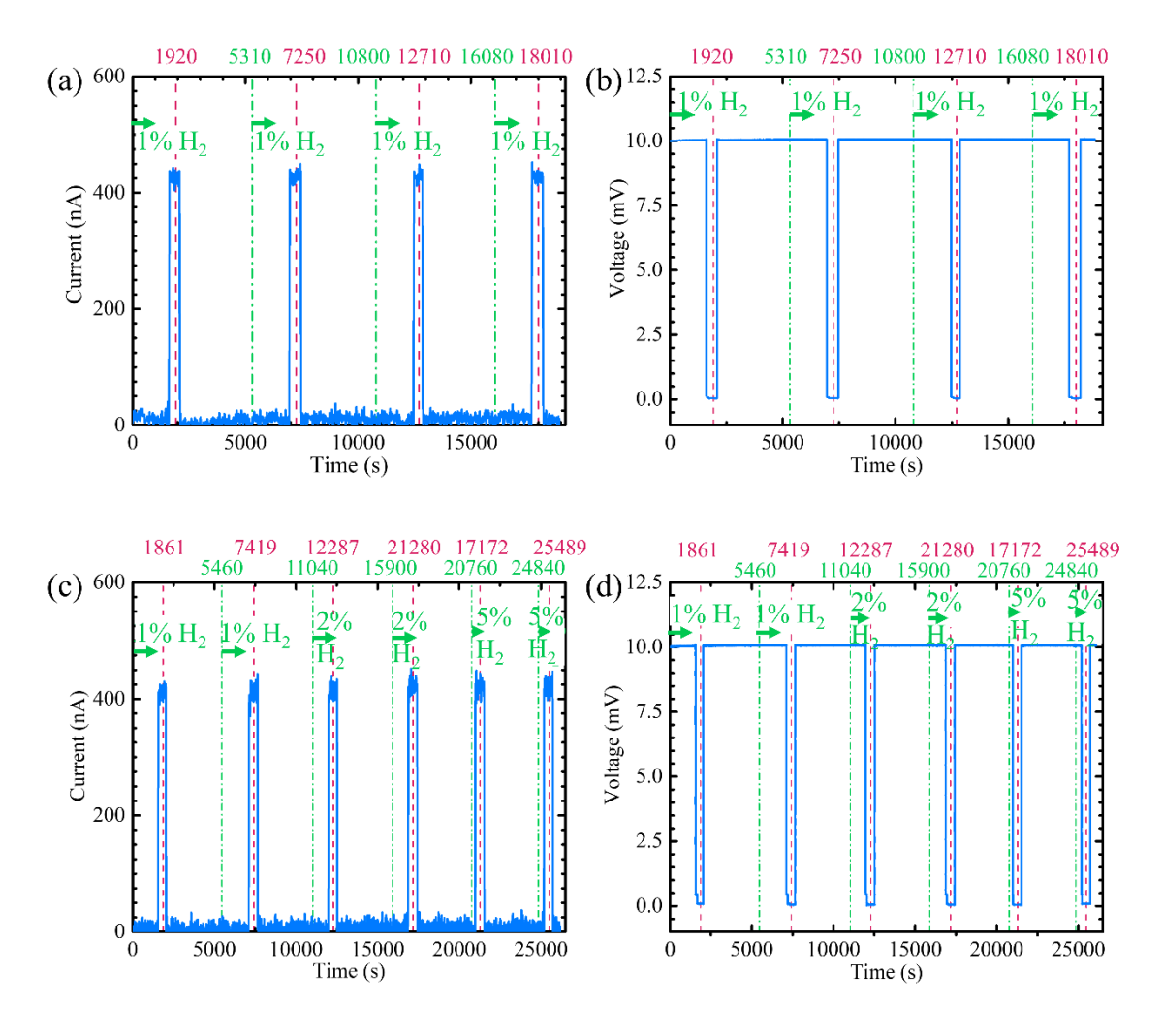


Figure 4: Temporal response of current (a, c) and voltage (b, d) for an event-driven sensor system composed of parallelly connected 50 μ m, 75 μ m, 100 μ m, and 125 μ m long cantilevers exposed to H₂ gas pulses. Panels (a) and (b) show the system's response to a pulse train at 1% H₂ concentration, while panels (c) and (d) present responses at 1%, 2%, and 5% H₂ in a balanced N₂ environment. The green dashed line marks the introduction of H₂ into the chamber, and the red dashed line indicates the termination of H₂ flow, followed by N₂ purging. The resulting current pulse train shows the sensor system's capability to generate wake-up signals.

Responsive materials

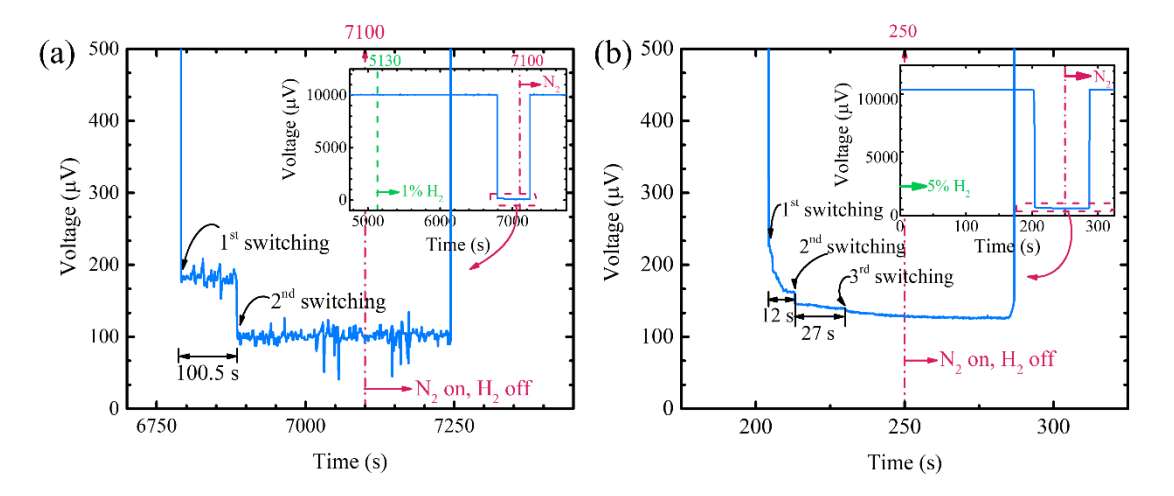


Figure 5: Temporal voltage drops response of the zero-standby power event-driven hydrogen sensor system under (a) 1% H₂ and (b) 5% H₂ concentrations. The sensor system comprises independent microcantilever-based switches, each with a distinct gap between the movable electrode and bottom electrode. This variation affects the closing time of the switches, depending on the hydrogen concentration in the target environment. The voltage drop across these parallel-connected switches provides a means to quantify the hydrogen concentration present.

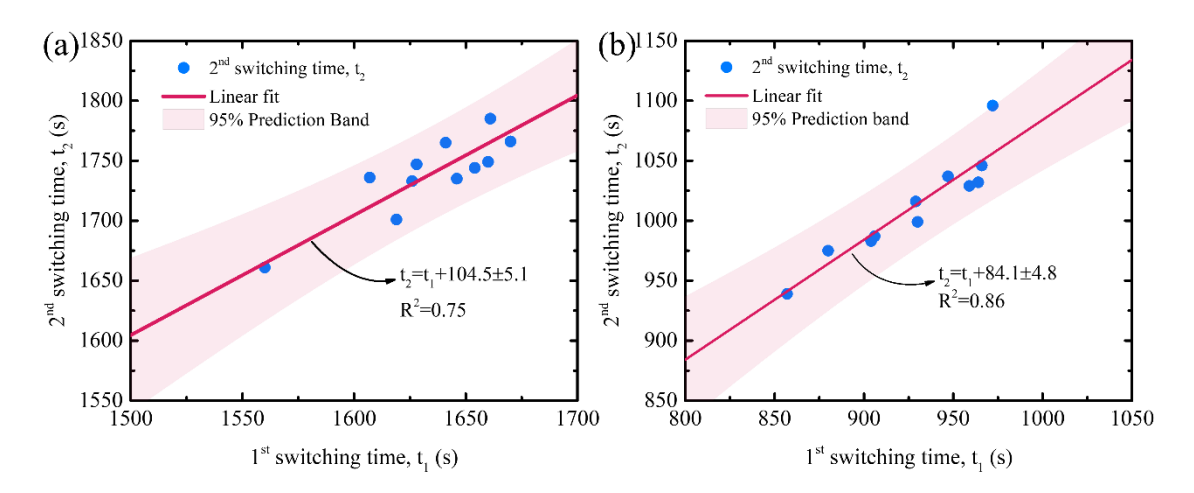


Figure 6: Correlation between the first and second switching events in the designed zero-standby power sensor system at (a) 1% and (b) 2% H_2 concentration in balanced nitrogen. The results indicate that the average time for the second switching event is 104.5 ± 5.1 s for 1% H_2 and 84.1 ± 4.8 s for 2% H_2 after the occurrence of the first switching event.

WILEY

RESPONSIVE MATERIALS

Supporting Information

Supporting Information is available from the Wiley Online Library.

Acknowledgements

S M J. N., Z. H., K. L., and X. W. acknowledge the support by NASA Grant Number

80NSSC23M0076. Z. H. acknowledges the support by NSF through the University of

Delaware Materials Research Science and Engineering Center, DMR-2011824. S. R. S.

acknowledges the support by NSF under award ECCS-2102027. The authors thank Dr.

Yuping Zeng and Dr. Nathan Lazarus for providing access to multimeters used in this

research.

Conflict of Interest

S M J. N. and X. W. are listed as inventors on a pending patent application by the University

of Delaware related to the system in this manuscript. The remaining authors declare no conflict

of interest.

Data Availability Statement

The data that support the findings of this study are available from the corresponding author

upon reasonable request.

ORCID (optional)

Received: ((will be filled in by the editorial staff))

Revised: ((will be filled in by the editorial staff))

Published online: ((will be filled in by the editorial staff))

18

References

- [1] S. Evro, B. A. Oni, O. S. Tomomewo, *International Journal of Hydrogen Energy* **2024**, 78, 1449.
- [2] K. Ramaiyan, L.-k. Tsui, E. L. Brosha, C. Kreller, J. R. Stetter, T. Russ, W. Du, D. Peaslee, G. Hunter, J. Xu, D. Makel, F. Garzon, R. Mukundan, *ECS Sensors Plus* **2023**, *2*, 045601.
- [3] B. Ai, Y. Sun, Y. Zhao, Small 2022, 18, 2107882.
- [4] R. Ramachandran, R. K. Menon, *International Journal of Hydrogen Energy* **1998**, *23*, 593.
- [5] L. Wen, Z. Sun, Q. Zheng, X. Nan, Z. Lou, Z. Liu, D. R. S. Cumming, B. Li, Q. Chen, Light: Science & Applications 2023, 12, 76.
- [6] A. Majumdar, J. M. Deutch, R. S. Prasher, T. P. Griffin, Joule 2021, 5, 1905.
- [7] W. Liu, H. Zuo, J. Wang, Q. Xue, B. Ren, F. Yang, *International Journal of Hydrogen Energy* **2021**, *46*, 10548.
- [8] C. A. Grimes, K. G. Ong, O. K. Varghese, X. Yang, G. Mor, M. Paulose, E. C. Dickey, C. Ruan, M. V. Pishko, J. W. Kendig, A. J. Mason, *Sensors* **2003**, *3*, 69.
- [9] S. J. Pearton, F. Ren, IEEE Instrumentation & Measurement Magazine 2012, 15, 16.
- [10] X. Wang, Y. Zhao, Q. Dong, C. Chu, F. Xue, C. Wang, J. Bai, *Responsive Materials* **2025**, *3*, e20240037.
- [11] T. Hübert, L. Boon-Brett, G. Black, U. Banach, Sensors and Actuators B: Chemical **2011**, 157, 329.
- [12] I. Darmadi, F. A. A. Nugroho, C. Langhammer, ACS Sensors 2020, 5, 3306.
- [13] I. Lundström, S. Shivaraman, C. Svensson, L. Lundkvist, *Applied Physics Letters* **1975**, *26*, 55.
- [14] M. Kumar, V. Bhatt, A. Kumar, J.-H. Yun, *Materials Letters* **2019**, *240*, 13.
- [15] Y. Wang, X. Jiang, Y. Xia, Journal of the American Chemical Society 2003, 125, 16176.
- [16] M. Kumaresan, M. Venkatachalam, M. Saroja, P. Gowthaman, *Journal of Materials Science: Materials in Electronics* **2020**, *31*, 8183.
- [17] C. Caucheteur, M. Debliquy, D. Lahem, P. Megret, *IEEE Photonics Technology Letters* **2008**, *20*, 96.
- [18] L. Huang, Z. Zhang, Z. Li, B. Chen, X. Ma, L. Dong, L.-M. Peng, ACS Applied Materials & Interfaces 2015, 7, 9581.
- [19] C. Tang, W. Jin, X. Xiao, X. Qi, Y. Ma, L. Ma, Sensors and Actuators B: Chemical **2025**, 424, 136889.
- [20] V. Jelicic, M. Magno, K. Chikkadi, C. Roman, C. Hierold, V. Bilas, L. Benini, in 2015 6th International Workshop on Advances in Sensors and Interfaces (IWASI), 2015, p. 271.
- [21] C. McConnell, S. N. Kanakaraj, J. Dugre, R. Malik, G. Zhang, M. R. Haase, Y.-Y. Hsieh, Y. Fang, D. Mast, V. Shanov, *ACS Omega* **2020**, *5*, 487.
- [22] S. Tang, W. Chen, H. Zhang, Z. Song, Y. Li, Y. Wang, Frontiers in Chemistry 2020, 8, 174.
- [23] X.-Y. Zhang, R.-H. Ma, L.-S. Li, L. Fan, Y.-T. Yang, S.-Y. Zhang, *Scientific Reports* **2021**, *11*, 2404.
- [24] S. Mandal, A. V. Marsh, H. Faber, T. Ghoshal, D. K. Goswami, L. Tsetseris, M. Heeney, T. D. Anthopoulos, *Nature Electronics* **2025**, *8*, 343.
- [25] C. Zhang, T. Ding, Responsive Materials 2024, 2, e20240024.
- [26] F. Xu, J. Ma, K. Hu, Z. Zhang, C. Ma, B.-O. Guan, K. Chen, *Sensors and Actuators B: Chemical* **2024**, *400*, 134875.
- [27] F. Xu, J. Ma, C. Li, C. Ma, J. Li, B.-O. Guan, K. Chen, *Molecules* **2023**, *28*, 6984.
- [28] Z.-D. Duan, Z.-J. Zhou, S. Zhu, W.-Q. Diao, Z. Liu, L. Fan, S.-Y. Zhang, L.-P. Cheng, X.-D. Xu, *Applied Physics Letters* **2023**, *123*, 172201.

- [29] S. J. McKeown, L. L. Goddard, in *Lab-on-Fiber Technology*(Eds. A. Cusano, M. Consales, A. Crescitelli, and A. Ricciardi), Springer International Publishing, Cham, **2015**, p. 181.
- [30] J. Burgués, S. Marco, Sensors 2018, 18, 339.
- [31] R. H. Olsson, C. Gordon, R. Bogoslovov, *Journal of Physics: Conference Series* **2019**, 1407, 012042.
- [32] Z. Qian, S. Kang, V. Rajaram, C. Cassella, N. E. McGruer, M. Rinaldi, *Nature Nanotechnology* **2017**, *12*, 969.
- [33] V. Rajaram, Z. Qian, S. Kang, N. E. McGruer, M. Rinaldi, in 2018 IEEE Micro Electro Mechanical Systems (MEMS), 2018, p. 17.
- [34] R. W. Reger, B. Barney, S. Yen, M. Satches, M. Wiwi, A. I. Young, M. A. Delaney, B. A. Griffin, in *2017 IEEE SENSORS*, Glasgow, UK, **2017**, p. 1.
- [35] C. Ghosh, S. H. Khan, S. J. Broadbent, H. C. Hsieh, S. Noh, A. Banerjee, N. Farhoudi, C. H. Mastrangelo, R. Looper, H. Kim, in *2017 IEEE SENSORS*, Glasgow, UK, **2017**, p. 1.
- [36] A. Risso, V. Rajaram, S. Kang, S. D. Calisgan, M. M. Pavese, Z. Qian, M. Rinaldi, *Scientific Reports* **2022**, *12*, 12603.
- [37] S. Rana, J. Mouro, S. J. Bleiker, J. D. Reynolds, H. M. H. Chong, F. Niklaus, D. Pamunuwa, *Nature Communications* **2020**, *11*, 1181.
- [38] R. Carpick, G. Wabiszewski, F. Streller, in *Solid State Sensors, Actuators and Microsystems Workshop*, Hilton Head Island, SC, USA, **2014**, p. 28.
- [39] H. Kam, V. Pott, R. Nathanael, J. Jaeseok, A. Elad, L. Tsu-Jae King, in 2009 IEEE International Electron Devices Meeting (IEDM), 2009, p. 1.
- [40] S. Mingoo, H. Scott, L. Yu-Shiang, F. Zhiyoong, K. Daeyeon, L. Yoonmyung, L. Nurrachman, D. Sylvester, D. Blaauw, in *2008 IEEE Symposium on VLSI Circuits*, **2008**, p. 188.
- [41] Y. Lee, S. Bang, I. Lee, Y. Kim, G. Kim, M. H. Ghaed, P. Pannuto, P. Dutta, D. Sylvester, D. Blaauw, *IEEE Journal of Solid-State Circuits* **2013**, *48*, 229.
- [42] W. Jiang, L. Wang, X. Wang, L. Zhao, X. Fang, R. Maeda, *Nanomaterials* **2022**, *12*, 3718.
- [43] F. Rahman, M. A. Salam Akanda, *Journal of Mechanical Science and Technology* **2022**, *36*, 4635.
- [44] S. J. Park, J. C. Doll, B. L. Pruitt, *Journal of Microelectromechanical Systems* **2010**, *19*, 137.
- [45] A. Basu, R. P. Hennessy, G. G. Adams, N. E. McGruer, *Journal of Micromechanics and Microengineering* **2014**, *24*, 105004.
- [46] Z. Huang, W. Wu, E. Herrmann, K. Ma, Z. A. Chase, T. A. Searles, M. B. Jungfleisch, X. Wang, *Frontiers of Optoelectronics* **2024**, *17*, 13.
- [47] H. Li, Y. Li, K. Wang, L. Lai, X. Xu, B. Sun, Z. Yang, G. Ding, *International Journal of Hydrogen Energy* **2021**, *46*, 1434.
- [48] F. Afshar, S. Nazarpour, A. Cirera, Journal of Applied Physics 2010, 108, 093513.
- [49] R. Treml, D. Kozic, J. Zechner, X. Maeder, B. Sartory, H. P. Gänser, R. Schöngrundner, J. Michler, R. Brunner, D. Kiener, *Acta Materialia* **2016**, *103*, 616.
- [50] Y. Shroff, Y. Chen, W. Oldham, *Journal of Vacuum Science & Technology B: Microelectronics and Nanometer Structures Processing, Measurement, and Phenomena* **2001**, *19*, 2412.
- [51] A. Zalineeva, S. Baranton, C. Coutanceau, G. Jerkiewicz, Langmuir 2015, 31, 1605.
- [52] B. Wang, L. Sun, M. Schneider-Ramelow, K.-D. Lang, H.-D. Ngo, *Micromachines* **2021**, *12*, 1429.
- [53] D.-H. Kim, S.-J. Kim, H. Shin, W.-T. Koo, J.-S. Jang, J.-Y. Kang, Y. J. Jeong, I.-D. Kim, *ACS Nano* **2019**, *13*, 6071.

- [54] C. Wadell, F. A. A. Nugroho, E. Lidström, B. Iandolo, J. B. Wagner, C. Langhammer, *Nano Letters* **2015**, *15*, 3563.
- [55] M.-S. Jo, K.-H. Kim, J.-S. Lee, S.-H. Kim, J.-Y. Yoo, K.-W. Choi, B.-J. Kim, D.-S. Kwon, I. Yoo, J.-S. Yang, M.-K. Chung, S.-Y. Park, M.-H. Seo, J.-B. Yoon, *ACS Nano* **2023**, *17*, 23649.
- [56] S. J. McKeown, X. Wang, X. Yu, L. L. Goddard, *Microsystems & Nanoengineering* **2017**, *3*, 16087.
- [57] F. A. A. Nugroho, I. Darmadi, L. Cusinato, A. Susarrey-Arce, H. Schreuders, L. J. Bannenberg, A. B. da Silva Fanta, S. Kadkhodazadeh, J. B. Wagner, T. J. Antosiewicz, A. Hellman, V. P. Zhdanov, B. Dam, C. Langhammer, *Nature Materials* **2019**, *18*, 489.
- [58] M. O. Kim, K. Lee, H. Na, D. S. Kwon, J. Choi, J. I. Lee, D. Baek, J. Kim, in 2013 Transducers and Eurosensors XXVII: The 17th International Conference on Solid-State Sensors, Actuators and Microsystems, 2013, p. 2576.
- [59] H. Yamazaki, Y. Hayashi, K. Masunishi, D. Ono, T. Ikehashi, *Journal of Micromechanics and Microengineering* **2018**, *28*, 094001.